



# Geoeffectiveness of Interplanetary Alfvén Waves. II. Spectral Characteristics and Geomagnetic Responses

Yimin Han<sup>1,2</sup> , Lei Dai<sup>1</sup> , Shuo Yao<sup>3</sup> , Chi Wang<sup>1</sup> , Walter Gonzalez<sup>1,4</sup>, Suping Duan<sup>1</sup> , Benoit Lavraud<sup>5,6</sup> , Yong Ren<sup>1</sup>, and Zhenyuan Guo<sup>1</sup>

<sup>1</sup> State Key Laboratory of Space Weather, National Space Science Center, Chinese Academy of Sciences, Beijing 100190, People's Republic of China  
[ldai@spaceweather.ac.cn](mailto:ldai@spaceweather.ac.cn)

<sup>2</sup> College of Earth and Planetary Sciences, University of Chinese Academy of Sciences, Beijing 100049, People's Republic of China

<sup>3</sup> School of Geophysics and Information Technology, China University of Geosciences (Beijing), Beijing 100083, People's Republic of China

<sup>4</sup> National Institute for Space Research (INPE), São José dos Campos, Brazil

<sup>5</sup> Laboratoire d'Astrophysique de Bordeaux, Université Bordeaux, CNRS, Pessac, France

<sup>6</sup> Institut de Recherche en Astrophysique et Planétologie, Université de Toulouse, CNRS, UPS, CNES, Toulouse, France

Received 2022 October 24; revised 2022 November 14; accepted 2022 November 15; published 2023 March 7

## Abstract

Using multipoint observations over 10 yr near 1 au, we investigate the spectra (5 minutes to 2 hr) of interplanetary Alfvén waves and the responses in the geomagnetic activities. We compute the two-point correlations of the wave magnetic field between the ACE and the THEMIS spacecraft, which are separated by  $\sim 200$  Earth radius ( $R_E$ ) in the solar wind. Alfvén waves associated with high two-point correlations exhibit steep spectra (spectra index  $\sim -1.63$ ). Such Alfvén waves occur mostly in slow-speed streams. By contrast, Alfvén waves with low two-point correlations exhibit flatter spectra (spectra index  $\sim -1.51$ ) with a relative enhancement of power above  $2 \times 10^{-4}$  Hz. The occurrence of Alfvén waves with low two-point correlations is more equally distributed between high-speed and low-speed streams. In general, interplanetary Alfvén waves show correlations with moderate geomagnetic responses in symmetric ring-current intensity, SuperMAG electrojet (SME), and Kp indices. Statistical analyses indicate that the Alfvén waves with flat spectra correspond to stronger responses in the geomagnetic indices than those with steep spectra, suggesting the importance of the tens of minutes (30–90 minutes) Alfvénic power spectra in the generation of SME/Auroral Electrojets. These observations may shed light on the response of the magnetosphere to fluctuating interplanetary magnetic field  $B_z$ .

*Unified Astronomy Thesaurus concepts:* [Planetary magnetospheres \(997\)](#); [Solar-terrestrial interactions \(1473\)](#); [Solar-planetary interactions \(1472\)](#)

## 1. Introduction

Interplanetary Alfvén waves show a high correlation between velocity and magnetic field variations (Belcher & Davis 1971; Denskat & Burlaga 1977). The amplitude of the wave magnetic field can be larger than the average magnetic field (Belcher et al. 1969; Belcher & Davis 1971; Denskat & Burlaga 1977). The large-amplitude Alfvén waves are spherically polarized, with the rotation of the perturbation magnetic field on the surface of the sphere (Tsurutani et al. 1994, 2018). Alfvén waves are observed in a broad interplanetary region (Bruno et al. 2006). High levels of Alfvén wave activity are often observed in the high-speed solar wind streams and on their edges (Belcher & Davis 1971; Tsurutani et al. 2011; Shi et al. 2015). Alfvén waves have also been investigated in the heliospheric current sheet (Dai et al. 2014; Li et al. 2020) and corotating interaction regions (CIRs; Tsurutani et al. 1994, 1995a, 1995b; Borovsky & Denton 2010).

The spectra of the Alfvénic fluctuations have been a subject of great interest. The timescale of Alfvén waves varies from minutes to  $>10$  hr (Belcher & Davis 1971; Smith et al. 1995). Power spectra of the Alfvénic magnetic field are shown to have a frequency dependence from  $f^{-1.5}$  to  $f^{-2.2}$  (Belcher & Davis 1971;

Tsurutani et al. 1990, 2018). The spectral index of interplanetary fluctuations evolves with heliocentric distance (Bavassano et al. 1982; Tu et al. 1989; Tu & Marsch 1995). Power-law spectra have also been identified for Alfvénic fluctuations in the upstream region of the Earth's bow shock (Tsurutani et al. 1990; Wang et al. 2015; Guarnieri et al. 2018).

Alfvén waves represent a considerable source of southward interplanetary magnetic field (IMF; Gonzalez et al. 1999; Zhang et al. 2014). The magnetic reconnection between the southward  $B_z$  of interplanetary Alfvén waves and the magnetic field of the magnetosphere are considered to drive geomagnetic activity (Tsurutani & Gonzalez 1987; Tsurutani et al. 1990; Gonzalez et al. 1999; Hajra et al. 2014a). During CIR and high-speed streams, Alfvén waves produce the high-intensity long-duration continuous Auroral Electrojet (AE) activity (Tsurutani & Gonzalez 1987; Hajra et al. 2013). Interplanetary Alfvén waves are shown to be correlated with the AE index (Tsurutani & Gonzalez 1987; Tsurutani et al. 1990; Gonzalez et al. 1999; Diego et al. 2005; Chian et al. 2006; D'Amicis et al. 2007; Guarnieri et al. 2018). Repetitive substorms are reported to occur every  $\sim 1$ –4 hr, associated with northward turnings of the Alfvénic IMF (Lee et al. 2006). Continuous Alfvén waves are inferred to extend the recovery phase of geomagnetic storms (Tsurutani et al. 2011; Raghav et al. 2018; Telloni et al. 2021).

Data from multiple spacecraft in the solar wind are often used to investigate the correlation of the magnetic field in the solar wind (Denskat & Burlaga 1977; Russell et al. 1980; Richardson et al. 1998; Richardson & Paularena 2001;



Original content from this work may be used under the terms of the [Creative Commons Attribution 4.0 licence](#). Any further distribution of this work must maintain attribution to the author(s) and the title of the work, journal citation and DOI.

Farrugia et al. 2005). The correlation of the magnetic field between multiple spacecraft may relate to information on the scales and evolution of the structure (Russell et al. 1980; Richardson & Paularena 2001; Farrugia et al. 2005). In this study, we provide multipoint observations of the spectra of the Alfvén waves and the geomagnetic response. The spectra and geomagnetic response of Alfvén waves are shown to depend on the two-point correlation between spacecraft.

The geomagnetic responses to interplanetary Alfvén waves are an important element in solar-wind–magnetosphere interaction. The southward  $B_z$  from Alfvén waves is quite unsteady compared to that in coronal mass ejection (CME)-driven storms. Fluctuating  $B_z$  components may drive intermittent magnetopause reconnection, resulting in time-dependent magnetosphere/ionosphere convection, and dynamical substorm activity (Kennel 1996; Gonzalez et al. 1999). The present study on the geomagnetic response to Alfvén waves may shed new light on the response of the magnetosphere to fluctuating IMF $B_z$  (e.g., Raab et al. 2016; Wang & Branduardi-Raymond 2018; Dai et al. 2020).

The remaining sections of the paper proceed as follows. In Section 2, we present the data and the instrumentation used in the study. Section 3 investigates the properties of spectra of Alfvén waves. The geomagnetic responses to the Alfvén waves are studied in Section 4. The results are summarized and discussed in Section 5.

## 2. Data and Instruments

This study uses data from the ACE, THEMIS-B (THB), and THEMIS-C (THC) in the solar wind near 1 au. The ACE is located around the L1 Lagrange point (about 220–250  $R_E$  upstream from Earth in the GSM X-axis). The X-GSM of THB and THC are  $\sim -30$ – $60 R_E$ . The magnetic field data are obtained from MAG/ACE with a 16 s resolution (Smith et al. 1998) and FGM/THEMIS in the spin resolution of about 3 s (Auster et al. 2008). The plasma data are obtained from SWEPAM/ACE with a 64 s resolution (McComas et al. 1998) and ESA/THEMIS in the spin resolution of about 3 s (McFadden et al. 2008). All the data used in our study are in the Geocentric Solar Magnetospheric (GSM) coordinates.

For the geomagnetic index, we use the symmetric ring-current intensity (SYM-H) index from the OMNI database. Dst and SYM-H are both indices to measure the intensity of the geomagnetic storm. SYM-H is essentially the same as the Dst index but with a high time resolution of 1 minute (Wanliss & Showalter 2006).

We use the SuperMAG electrojet (SME) indices, which is a generalized version of the AE indices (Newell & Gjerloev 2011). Similarly, SMU and SML are the SuperMAG version of AU and AL, respectively. SME indices (SMU, SML) are at a 1 minute cadence and calculated with data from more than 100 stations. SMU/AU and SML/AL represent a measure of maximum eastward and westward AE current, respectively.  $SME/AE = SMU/AU - SML/AL$  represents a measure of the maximum AE current in the high-latitude ionosphere.

We use the 3 hr Kp index from the GFZ German Research Center for Geosciences (Matzka et al. 2021). The Kp is derived from 13 geomagnetic stations between 44° and 60° geomagnetic latitude. The Kp index ranges from 0–9 and is given in units of 1/3.

## 3. Multipoint Observation of Interplanetary Alfvén Waves

### 3.1. Alfvén Wave Events

Figure 1 provides an overview of the Alfvén wave events on 2011 February 8 and 2014 August 31. The solar wind speed is around  $\sim 400$ – $450 \text{ km s}^{-1}$  during these time intervals (Figure 1(a), (d)). The THEMIS data is time shifted to the location of ACE. The time shift is estimated by finding the amount of time delay that corresponds to the maximal correlation of 6 hr intervals of  $B_z$  between ACE and THEMIS. For these two events, the time delay from ACE to THEMIS is roughly 1 hr considering the solar wind speed and the separation of about  $\sim 200 R_E$  between ACE and THEMIS. We obtain  $\delta B_z$  (or  $\delta V_z$ ) by subtracting the 6 hr running average  $B_z$  (or  $V_z$ ) from the original  $B_z$  (or  $V_z$ ). In each event, the  $\delta B_z$  and  $\delta V_z$  components exhibit a strong ( $>0.8$ ) correlation (Figures 1(b), (c), (e), (f)). In our study, Alfvén waves are identified by high correlations ( $>0.8$ ) between  $\delta V_z$  and  $\delta B_z$  in 6 hr intervals (Belcher & Davis 1971). Notice that the correlation between  $\delta B$  and  $\delta V$  may significantly vary in high-speed streams and CIRs (Tsurutani et al. 1995b, 2011).

The Alfvén waves in the two events show significant differences. In the 2011 February 8 event, the  $\delta B_z$  has a high correlation ( $\approx 0.901$ ) between ACE and THB as shown in Figures 1(b) and (c). THB observes almost the same waveform of  $B_z$  as the Alfvén waves are convected by the solar wind from ACE to THB. In the 2014 August 31 event, however, ACE and THB observed distinctly different  $B_z$  waveforms. The correlation of  $\delta B_z$  between ACE and THB is weak ( $\approx 0.325$ ).

Previous studies from ISEE spacecraft suggest that small-scale IMF structures may have low correlations over the distance of  $\sim 200 R_E$  (Russell et al. 1980; Tsurutani et al. 1990; Guarnieri et al. 2018). Fluctuations of small-wavelength are more likely to evolve and decorrelate over a certain distance ( $\sim 200 R_E$ ) (Russell et al. 1980; Richardson & Paularena 2001; Farrugia et al. 2005). Hence, the two-location correlation may reflect some information regarding the scales or evolution of Alfvén waves. The observations in Figure 1 motivate us to classify and analyze Alfvén waves using the two-point correlation in the solar wind in the next section.

### 3.2. Statistical Study of the Alfvén Waves' Spectra

The database for the statistical study consists of ACE and THEMIS data from 2010 October to 2020 October. THB and THC are mostly in the solar wind but occasionally traverse the Earth's magnetosphere. Two criteria are applied to ensure THB and THC are in the interplanetary space: the proton number density is less than  $50 \text{ cm}^{-3}$  and the proton velocity is more than  $200 \text{ km s}^{-1}$ . The intervals when the two THEMIS spacecraft are located in the lunar shadow are also excluded (Sibeck et al. 2011).

We divide ACE and THEMIS data into samples of 6 hr intervals. ACE and THEMIS satellites move less than  $\sim 15 R_E$  during a 6 hr interval. The spacecraft motion is much less than the ACE-THEMIS separation of  $\sim 200 R_E$ . Thus, ACE and THEMIS are treated as stationary in each 6 hr interval. The data from THEMIS are time shifted to ACE as described in the event study. The magnetic field and velocity data are all interpolated to the same (64 s) time resolution. Each 6 hr interval is identified as an Alfvén wave event if the absolute value of the correlation between  $\delta B_z$  and  $\delta V_z$  is larger than 0.8. This criterion for Alfvén waves is consistent with previous

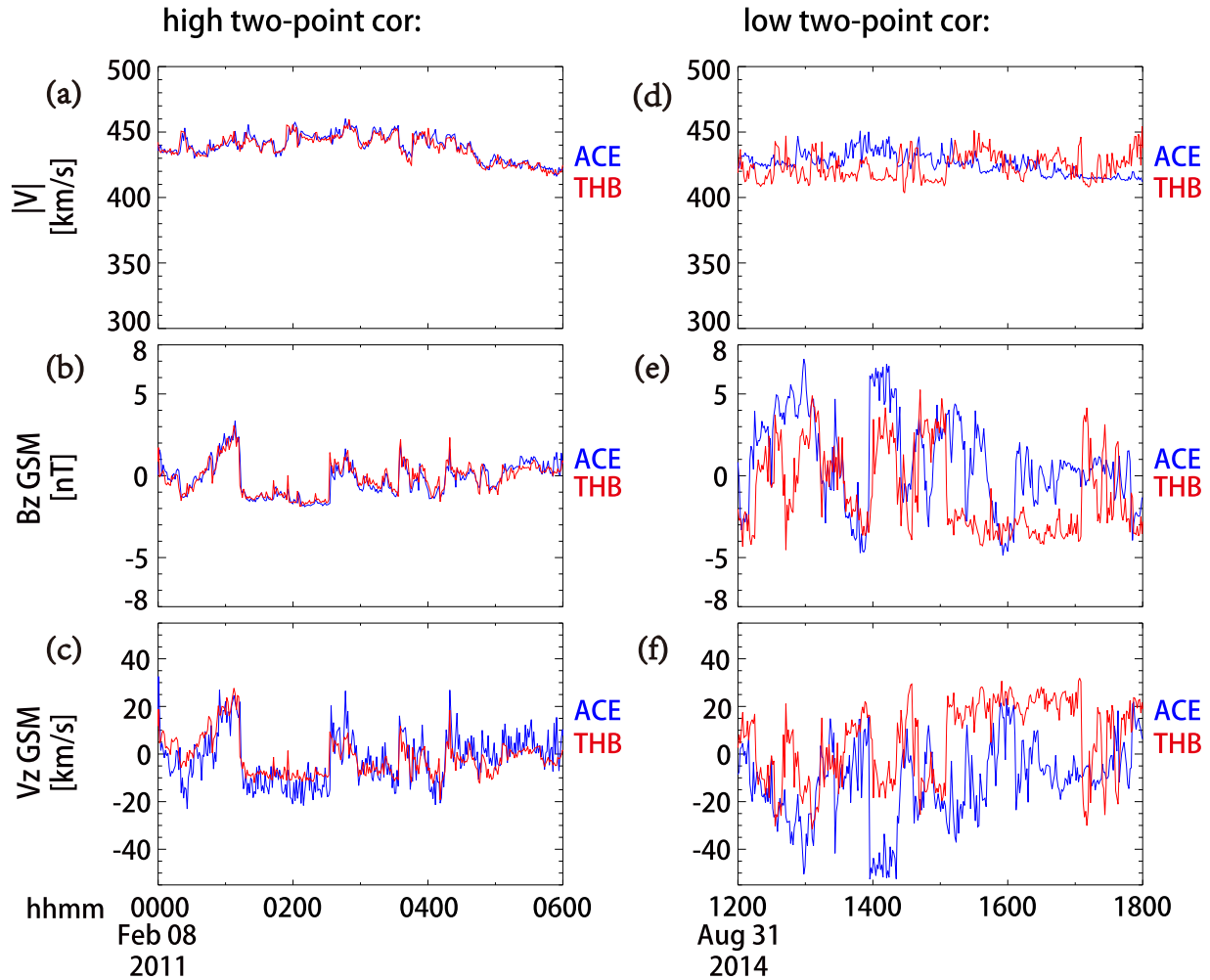


**Figure 1.** Two events of interplanetary Alfvén waves observed by ACE and THB on 2011 February 8 (left) and 2014 August 31 (right). (a), (d) Solar wind velocity  $|V|$  from ACE (blue) and THB (red). (b), (e)  $\delta B_z$  in GSM from ACE and THB. (c), (f)  $\delta V_z$  in GSM from ACE and THB.

studies (Belcher et al. 1969; Tsurutani et al. 1990; Shi et al 2015). We find a total of 2346 samples of events of Alfvén waves encountered by both ACE and THEMIS spacecraft.

For each event of Alfvén waves, we compute the two-point correlation of  $\delta B_z$  between ACE and THEMIS. The distribution of the two-point correlation is shown in Figure 2(a). We categorize the Alfvén waves into three types: the high two-point correlation ( $>0.8$ , orange) type, the medium two-point correlation ( $0.5 \sim 0.8$ , blue) type, and the low two-point correlation ( $<0.5$ , black) type. We obtained 577, 1238, and 531 samples for the three types of Alfvén waves, respectively.

For each event sample, a power spectral density (PSD) is generated by applying the standard fast Fourier transform analysis. Figures 2(b) and (c) present the spectra for each type of Alfvén wave.

The average PSD of the Alfvén waves is shown in Figure 2(b). A power-law fitting is performed in the frequency range of  $1.39 \times 10^{-4}$  to  $3.24 \times 10^{-3}$  Hz (5.1 minutes to 2 hr). The spectral slopes exhibit a variation from  $-1.624$  to  $-1.497$  for the three types. The low two-point correlation (black) Alfvén waves correspond to a spectrum of  $f^{-1.497}$ . By contrast, the high two-point correlation (orange) Alfvén waves correspond to a steeper spectrum of  $f^{-1.624}$ . The spectrum of the medium-correlation type has an intermediate index close to

$-1.530$ . Notice that the low two-point correlation Alfvén waves contain more power as compared with the high-correlation Alfvén waves in the frequency range  $>3 \times 10^{-4}$  Hz.

Figure 2(c) shows the median value of the PSD for each type of Alfvén wave. The spectral slopes of the low-correlation, medium-correlation, and high-correlation types are  $f^{-1.508}$ ,  $f^{-1.546}$ , and  $f^{-1.633}$ , respectively. The characteristics of the median spectra are consistent with those of the average spectra, indicating that the statistical results are not dominated by extreme events.

We compute the spectral slope  $\alpha$  of each event and show the distribution in Figure 3. This provides an alternative measurement of the spectral index of Alfvén waves. The spectral index for a single event varies in a broad range in the 2346 events. The distribution of spectral indices is distinctly different for the high two-point correlation type and low two-point correlation type. The spectral slopes are steeper for the high two-point correlation type. These results are consistent with the statistical results shown in Figures 2(b) and (c).

The statistical results shown in Figures 2 and 3 indicate a dependence of spectral properties of Alfvén waves on the two-point correlation. One effect that may contribute to this dependence is the evolution and propagation of small-scale Alfvén waves during the convection from ACE to THEMIS. It

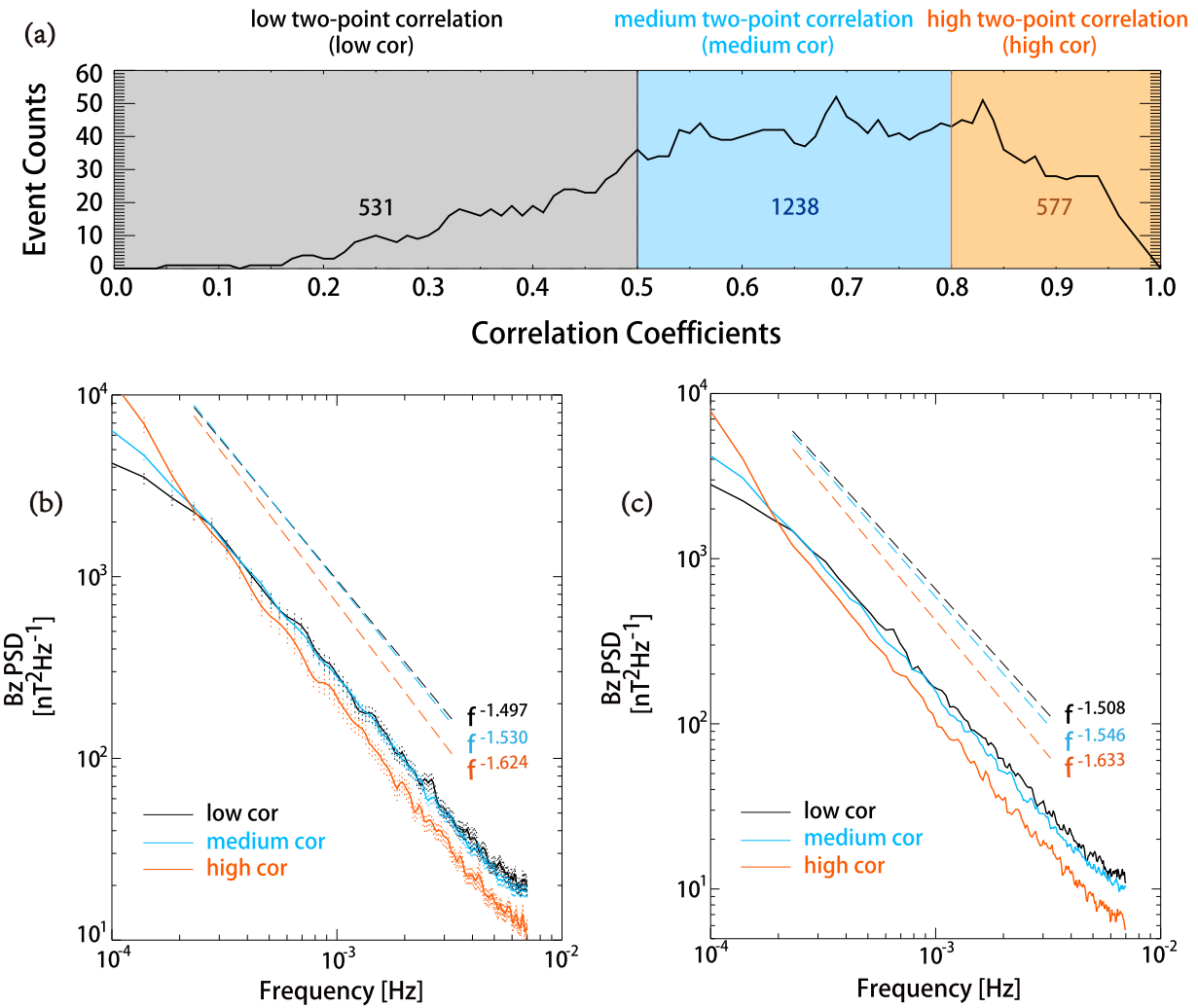


**Figure 2.** The two-point correlation and the power spectra of Alfvén waves. (a) The distribution of the absolute value of the two-point correlation coefficients of  $\delta B_z$  between ACE and THEMIS. (b) The average spectra of  $\delta B_z$  of the Alfvén waves from ACE for the low two-point correlation (black), the medium two-point correlation type (blue), and the high two-point correlation type (orange). The vertical ranges represent the 95% confidence limits. (c) The median spectra of  $\delta B_z$  of the Alfvén waves from ACE. The power-law fits are shown as dashed lines.

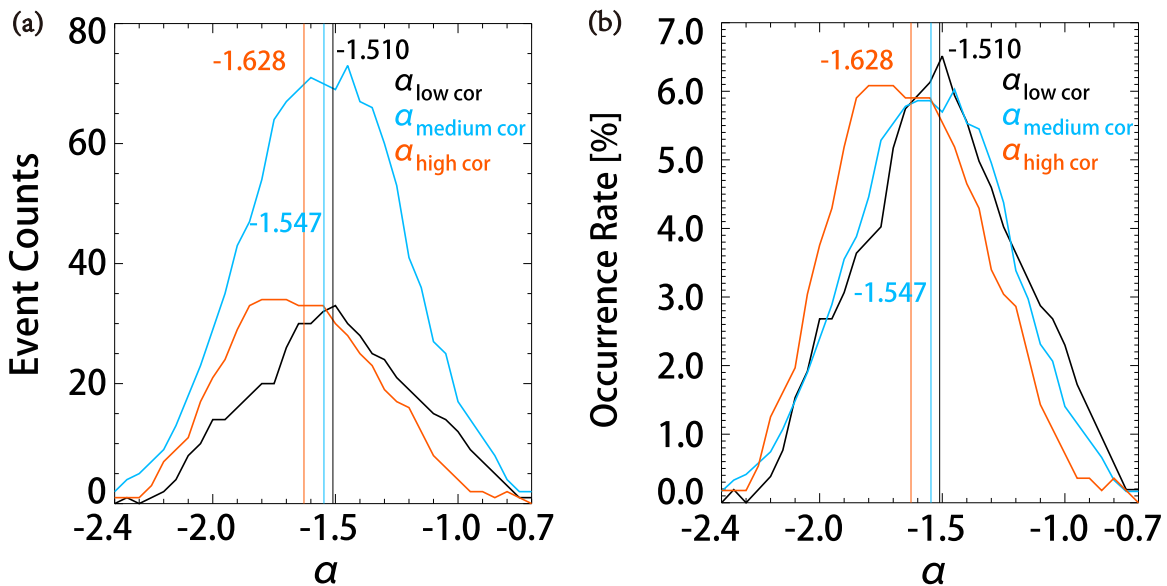


**Figure 3.** The spectral indices  $\alpha$  of the low two-point correlation (black), medium two-point correlation (blue), and high two-point correlation (orange) types of Alfvén waves events from ACE. (a) The distribution of the spectral indices associated with Alfvén wave events. (b) The occurrence rate of the spectral indices associated with Alfvén wave events. Mean values are shown with the vertical lines.



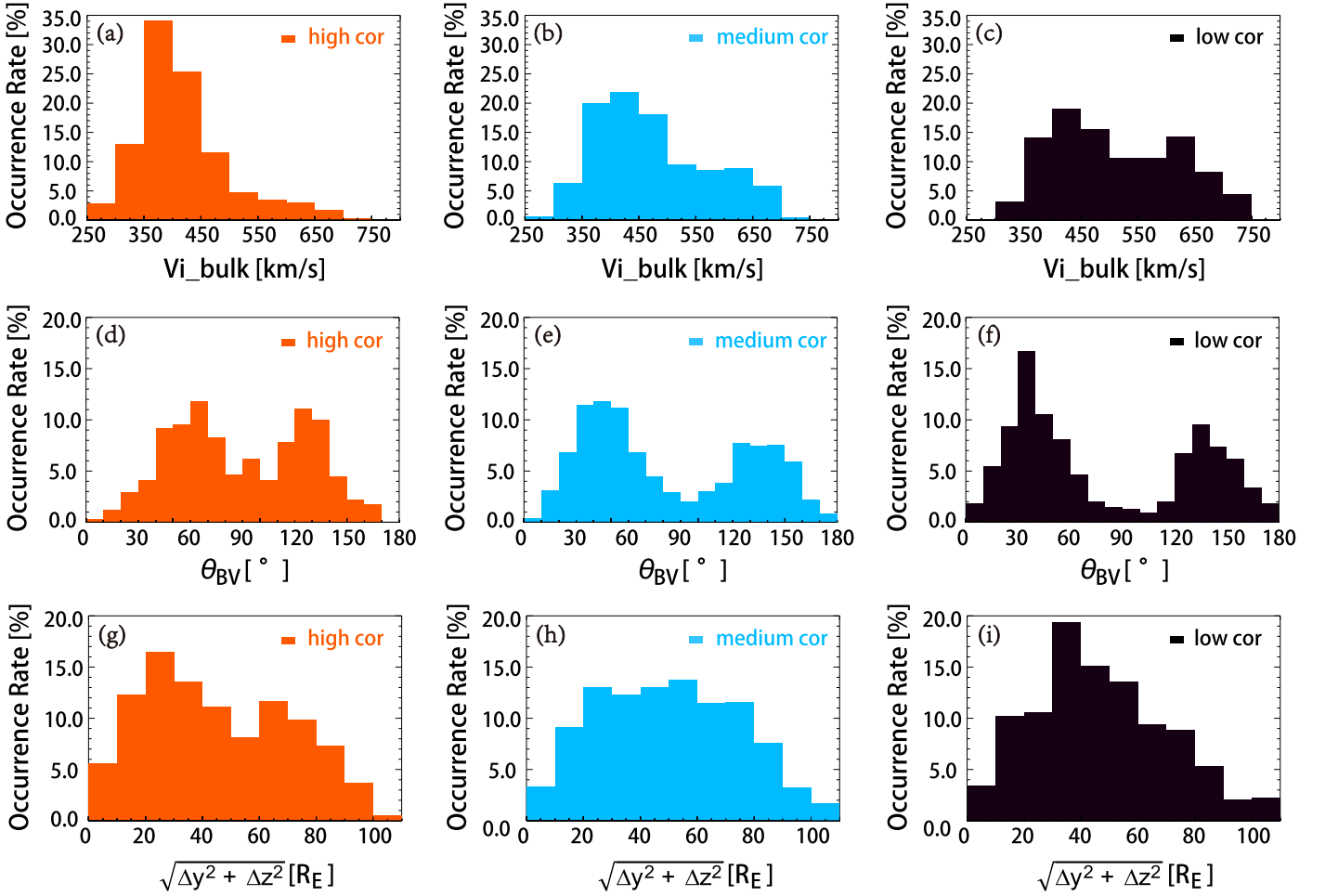


**Figure 4.** Statistical distributions of the solar wind speed, the  $\theta_{BV}$  between velocity and magnetic field, and spacecraft separations associated with the Alfvén waves. (a)–(c) The occurrence rate of the solar wind speed from ACE associated with the Alfvén waves. (d)–(f) The occurrence rate of the  $\theta_{BV}$  from ACE associated with the Alfvén waves. (g)–(i) The occurrence rate of the deviations  $\sqrt{\Delta y^2 + \Delta z^2}$  between ACE and THEMIS.

takes  $\sim 1$  hr for the solar wind to convect ( $\sim 400 \text{ km s}^{-1}$ ) over  $\sim 200R_E$  from ACE to THEMIS satellites. During the convection, the Alfvénic fluctuations evolve and propagate in the rest frame of the solar wind (Bruno et al. 2003). For our events, the convection time of  $\sim 1$  hr is comparable to or larger than the timescale of small-scale ( $< 1$  hr or  $> 3 \times 10^{-4}$  Hz) Alfvén waves. Those small-scale fluctuations are expected to evolve significantly and cause de-correlation over the  $\sim 200R_E$  distance. The above scenario is in particular supported by observations of the magnitude of the power spectra at  $> 2 \times 10^{-4}$  Hz ( $< 90$  minutes) shown in Figures 2(b) and (c). The relative enhancement of power at  $> 2 \times 10^{-4}$  Hz ( $< 90$  minutes) is likely related to the decrease in the two-point correlation (black and blue curves). By contrast, Alfvén waves that have a high two-point correlation contain less wave power at a timescale of less than 90 minutes.

### 3.3. Statistical Characteristics during the Alfvén Waves

We present the distribution of the solar wind speed for the three types of Alfvén waves in Figures 4(a)–(c). More than 75% of the high two-point correlation events are in the slow solar wind range (250–450  $\text{km s}^{-1}$ ). In contrast, the low two-point correlation events are more equally distributed in the high-speed and slow-speed streams (Figure 4(c)). The spectra slope ( $\sim -1.63$ ) of the high two-point correlation Alfvén waves

is close to  $-5/3$ . This feature is consistent with the suggestion that fluctuations in slow streams represent fully developed turbulence with spectra close to  $f^{-5/3}$  (Tu et al. 1989; Horbury et al. 2005). In the fast solar wind, the spectra may evolve depending on radial distance (Bavassano et al. 1982; Denskat & Neubauer 1982). This effect may contribute to the small deviation from  $f^{-5/3}$  spectra in the low two-point correlation Alfvén waves.

In the solar wind, the power spectra measured by a single spacecraft is a reduced spectrum (Bieber et al. 1996; Horbury et al. 2005). It has been suggested that the reduced spectrum depends on the angle ( $\theta_{BV}$ ) between the magnetic field vector and the solar wind flow direction (Bieber et al. 1996; Horbury et al. 2008). Figures 4(d)–(f) display the distribution of  $\theta_{BV}$  associated with Alfvén waves.  $\theta_{BV}$  are more concentrated in the range of  $60^\circ \pm 20^\circ$ ,  $90^\circ$ – $100^\circ$ , and  $110^\circ$ – $140^\circ$  in the high-correlation Alfvén waves ( $\sim 74\%$ ). In contrast, the flow direction is more aligned with  $\mathbf{B}$  for the low two-point correlation type (Figure 4(f)). The  $\theta_{BV}$  effect may also contribute to the difference between the spectra indices.

We present the distribution of  $\sqrt{\Delta y^2 + \Delta z^2}$  between the two satellites during each event in Figures 4(g)–(i). This spacecraft separation in principle may significantly affect the two-point correlation. For both high two-point correlation and low two-point correlation events, a 10%–15% occurrence rate

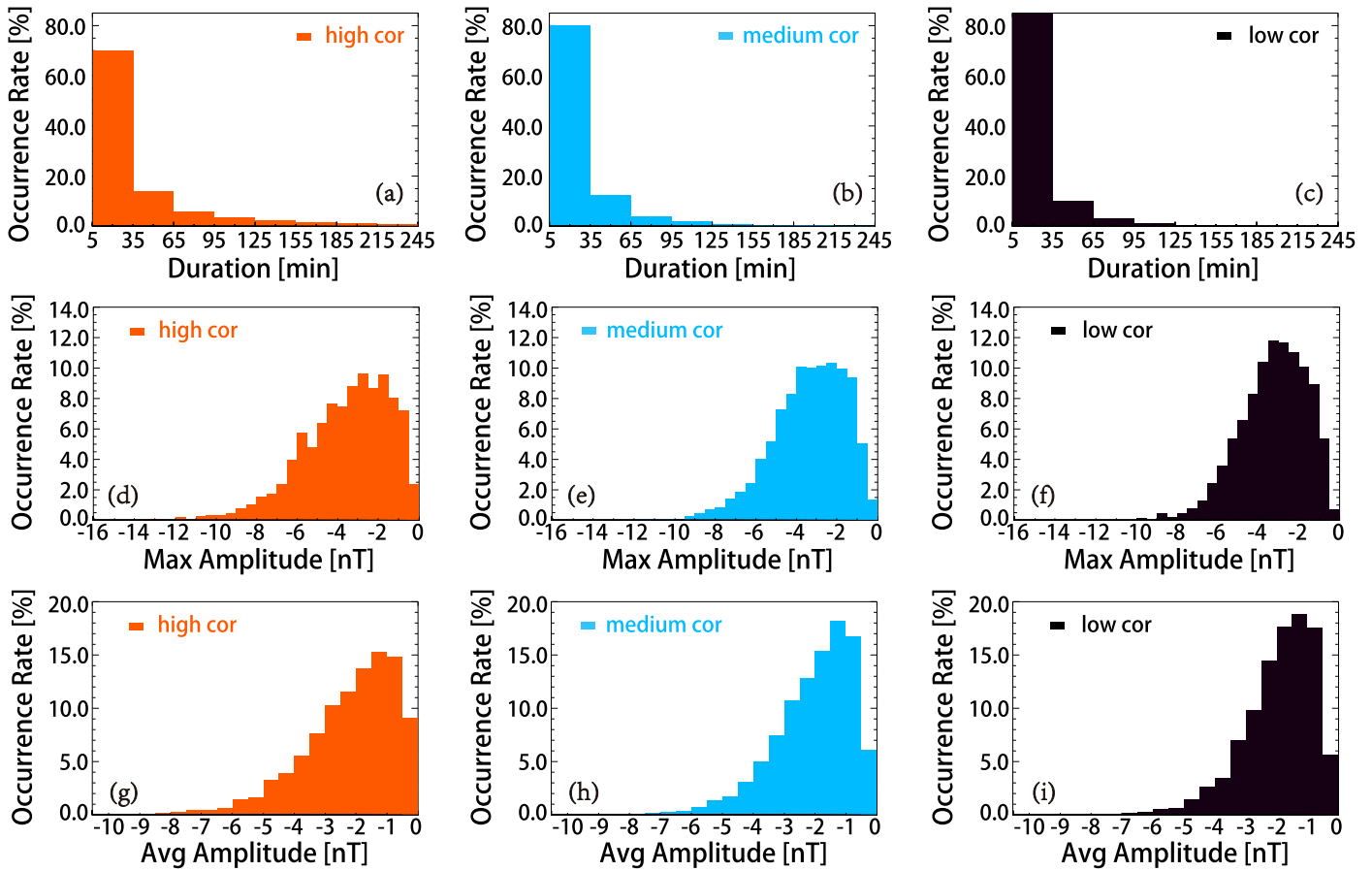


**Figure 5.** Statistical distributions of the southward  $B_z$  during the Alfvén waves. (a)–(c) The occurrence rate of the duration of the IMF southward  $B_z$  associated with the Alfvén waves. (d)–(f) The occurrence rate of the maximum southward  $B_z$  associated with the Alfvén waves. (g)–(i) The occurrence rate of the average southward  $B_z$  associated with the Alfvén waves.

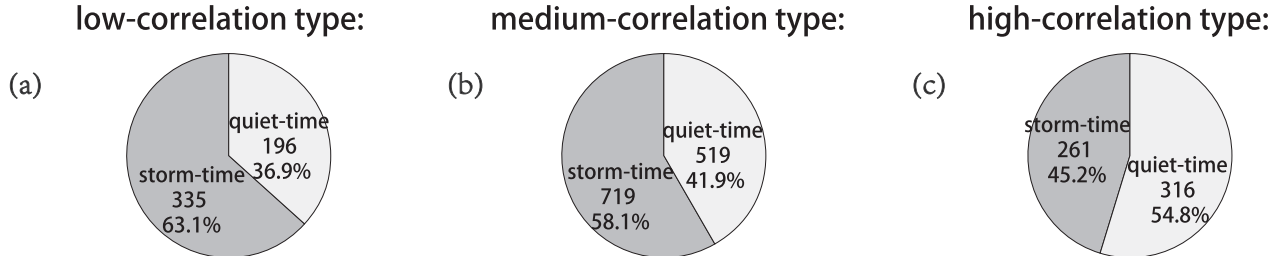


**Figure 6.** Storm time and non-storm time distribution of the Alfvén waves events from 2010 October to 2020 October. (a) the distribution of Alfvén waves with low two-point correlations. (b) The distribution of Alfvén waves with medium two-point correlations. (c) The distribution of Alfvén waves with high two-point correlations.

is nearly equally distributed from 10–80  $R_E$ . No significant difference is found as shown in Figures 4(g)–(i). The observations suggest that the spacecraft separation does not significantly affect the two-point correlation in the statistical study.

Figure 5 shows statistical distributions of the southward  $B_z$  during the Alfvén waves. The duration of southward  $B_z$  is mostly less than 60 minutes. The occurrence rate for the short-duration  $B_z$  (less than 35 minutes) is the largest for the low two-point correlation type. This feature is consistent with the results in Figure 2 showing an enhancement of power at  $<1$  hr for the low two-point correlation events. The average amplitude of southward  $B_z$  is mostly distributed in the range of  $-1$  to  $-6$  nT, as shown in Figures 5(d)–(f) and Figures 5(g)–(i). The average of the maximum is  $-3.25$  nT for the low two-point correlation

events (black) and  $-3.58$  nT for the high two-point correlation events (orange). On average, the distributions of the maximum and average southward  $B_z$  are more toward larger values in the high two-point correlation events (orange) as compared to those in the low two-point correlation events (black).

#### 4. Geomagnetic Responses to Interplanetary Alfvén Waves

In this section, we use the SYM-H, SME, and Kp indices from 2010 October to 2020 October to investigate the geomagnetic responses to interplanetary Alfvén waves.

Using the method in Dai et al. (2015a), we sort Alfvén waves into storm time and quiet (non-storm) time events. Geomagnetic storms are included if SYM-H reaches a minimum of  $-30$  nT in the main phase (Gonzalez et al. 1994). Among the total

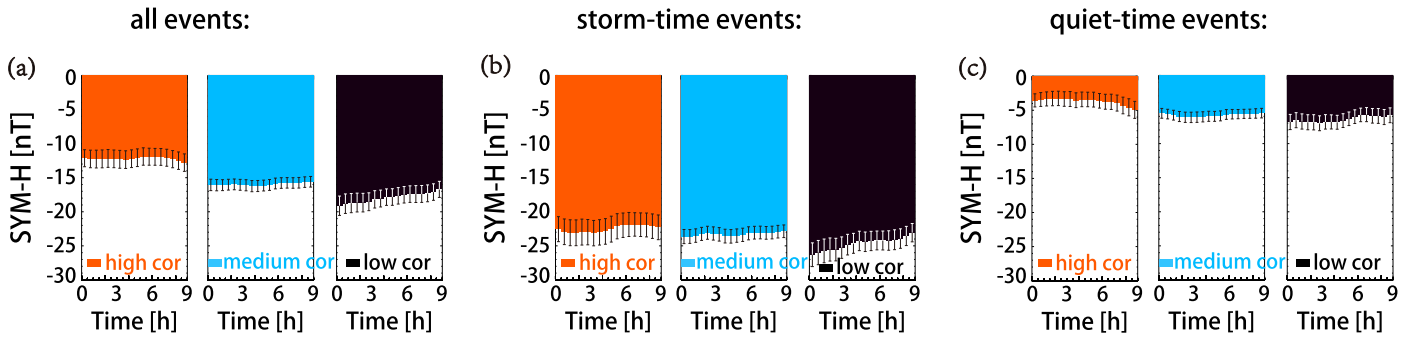


**Figure 7.** The response of the SYM-H index to Alfvén waves from 2010 October to 2020 October. The average value of the SYM-H index associated with (a) all events, (b) storm time events, and (c) non-storm time events for low two-point correlation (black), medium two-point correlation (blue), and high two-point correlation (orange) type Alfvén waves. Vertical ranges represent the 95% confidence limits.

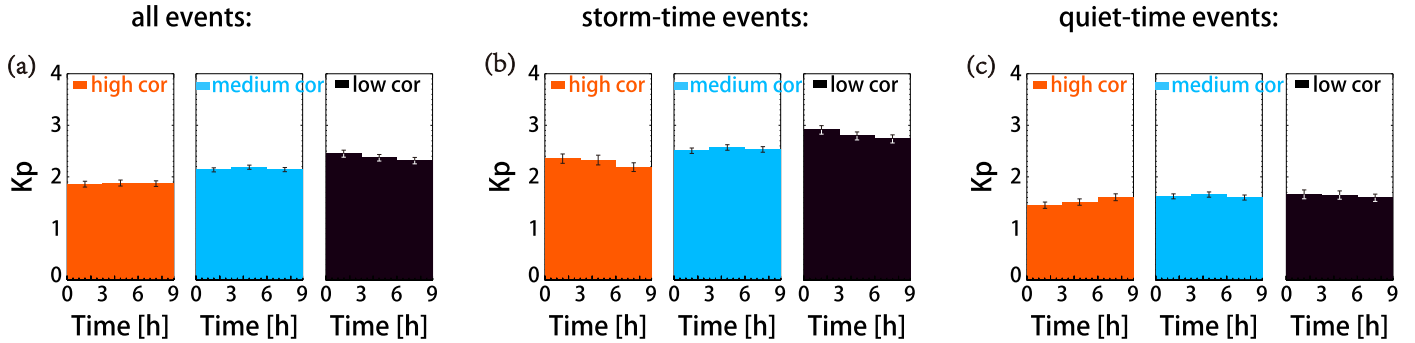


**Figure 8.** The response of the Kp index associated with Alfvén waves from 2010 October to 2020 October. The average value of the Kp index associated with (a) all events, (b) storm time events, and (c) non-storm time events for low two-point correlation (black), medium two-point correlation (blue), and high two-point correlation (orange) type Alfvén waves. Vertical ranges represent the 95% confidence limits.

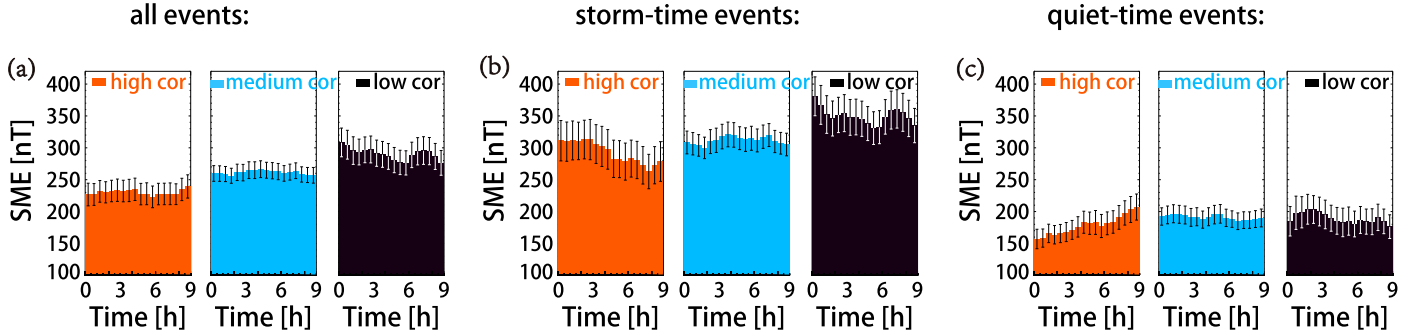


**Figure 9.** The response of the SME index associated with Alfvén waves from 2010 October to 2020 October. The average value of the SME index associated with (a) all events, (b) storm time events, and (c) non-storm time events for low two-point correlation (black), medium two-point correlation (blue), and high two-point correlation (orange) type Alfvén waves. Vertical ranges represent the 95% confidence limits.

2346 events, there are 1315 storm time events and 1031 quiet time events. As shown in Figures 6(a)–(c),  $\sim 63\%$  of the low two-point correlation type Alfvén waves are storm time events. In comparison, only  $\sim 45\%$  of the high two-point correlation type Alfvén waves are during storms.

We present the analysis of the response of the SYM-H index in Figure 7, the Kp index in Figure 8, and the SME index in Figure 9. The beginning of the 6 hr interval when THB/C observes the Alfvén waves is approximately treated as the arrival time (with an uncertainty of  $\sim 10$  minutes) of the Alfvén waves at the magnetopause. For each Alfvén wave event, we expect that the geomagnetic response to Alfvén waves is mostly within 9 hr with respect to the beginning of the event. This is because the interval of Alfvén waves is 6 hr and the response of substorm cycles is most likely within an additional 3 hr.

Figure 7 shows the response of the SYM-H index associated with Alfvén waves of different two-point correlations. In general, the SYM-H index is  $-12$  to  $-19$  nT in response to Alfvén waves (Figure 7(a)). The response in SYM-H is mostly contributed by Alfvén waves during the recovery phase of the storms, as indicated by an average of SYM-H of  $-22$  to  $-26$  nT in Figure 7(b). This observation is consistent with previous studies suggesting that Alfvén waves contribute to injections of particles into the ring current and the prolonged recovery phase of small storms (Kamide et al. 1998; Tsurutani et al. 2011; Telloni et al. 2021). During the non-storm time, the response of the SYM-H index is on average on the order of a few nanotesla. The Alfvén waves with low two-point correlations (black) are found to have the strongest response in the SYM-H index.

Figure 8 shows the Kp index in response to Alfvén waves. Kp is an index that monitors sub-auroral geomagnetic

disturbances on a global scale. On average, Alfvén waves correspond to a response of 2.0 in Kp (Figure 8(a)). Similar to the observation in the SYM-H index, the response of the Kp index is mostly contributed by the storm time Alfvén waves as large as 2.3–2.6 (Figure 8(b), (e)). The average response of the Kp index in quiet time is less than 1.66. The Alfvén waves with low two-point correlations (black) are found to have the strongest Kp response as large as 2.6–3 during storm time events.

Figure 9 shows the response of the SME index in response to the Alfvén waves. On average, all Alfvén waves correspond to a response in SME of  $\sim 230$ – $300$  nT (Figure 9(a)). Similar to the observations of SYM-H, the responses in SME are stronger ( $\sim 250$ – $350$  nT) in the storm time events. The responses in the non-storm time events are  $\sim 150$ – $200$  nT and also non-negligible.

The average response of SME indicates that Alfvén waves have a general relation with moderate AE activities. As shown in the in situ observations in our accompanying Paper I (Dai et al. 2023), the connection between Alfvén waves and AE increases is made possible by dayside magnetopause reconnection. The observations of the SME index suggest that Alfvén waves generally drive enhanced magnetosphere/ionosphere convection through transient magnetopause reconnection. The enhanced convection then causes enhanced current flow in the AEs and an associated growth of the AE index, which is typical in the substorm growth phase (Baumjohann & Treumann 1996; Kamide & Kokubun 1996).

The typical peak values of SME are generally  $>300$  nT during the substorm expansion phase (e.g., Zong et al. 2021). In our observations, the average response of SME is not large compared with this value. One possible reason is that the SME indices are averaged over the growth phase and non-substorm time (e.g., intervals of northward  $B_z$  in interplanetary Alfvén waves). Such an average may reduce the average response of the SME. Another possible reason is that Alfvén waves may not have a one-to-one relation to substorms, especially during the non-storm time. First, not all southward  $B_z$  of Alfvén waves may drive transient magnetopause reconnection. If the magnetosheath plasma-beta is large, Alfvén waves may need to produce a very large magnetic shear angle across the magnetopause to induce magnetic reconnection (Swisdak et al. 2003; Phan et al. 2013; Koga et al. 2019). Second, magnetopause reconnection induced by Alfvén waves drives enhanced convection and accordingly the increase of the convection electrojets component of SME/AE (Baumjohann & Treumann 1996; Kamide & Kokubun 1996). However, the enhanced convection may not have a one-to-one relation with substorm expansion and the substorm electrojet (Pytte et al. 1978; Baumjohann & Treumann 1996; Kamide & Kokubun 1996; Tsurutani et al. 2004). As a result, only a portion of interplanetary Alfvén waves may finally lead to substorm expansion and associated large increases in SME/AE.

Consistent with observations of SYM-H and Kp, Figures 9(a)–(c) indicate that Alfvén waves with low two-point correlations (black) have the strongest response in the SME index. Alfvén waves with low two-point correlations have more wave power at timescales of 30–90 minutes, suggesting that the Alfvénic power in this range may be important for driving SME activity. The Alfvénic power with short periods ( $<15$  minutes) probably have negligible geoeffectiveness (Tsurutani et al. 1990; Guarnieri et al. 2018). On

the other hand, long-duration ( $>2$  hr) southward  $B_z$  from Alfvén waves only represents a very small portion of all samples (Figure 5). Alfvén waves with  $B_z$  duration  $<2$  hr appear to be typical for causing AE activity (Tsurutani et al. 1995a). Notice that the 30–90 minute timescale is comparable to the typical 30–60 minute duration of substorm expansion. This coincidence is worth further in-depth investigations.

We also notice that Alfvén waves with low two-point correlations are not associated with larger  $B_z$  as compared with those with high two-point correlations. This suggests that the magnitude of  $B_z$  may not be the most important factor for the magnetopause reconnection. For instance, the magnitude of  $B_z$  of interplanetary Alfvén waves could be amplified by a factor of  $\sim 3$ – $6$  by the transmission through the bow shock as shown in our accompanying Paper I (see also McKenzie & Westphal 1969; Lu et al. 2009).

## 5. Conclusions and Discussion

Using 10 yr of data from ACE, THEMIS, and geomagnetic indices, we investigate the characteristics of the spectra of Alfvén waves and associated geomagnetic responses. The spectra of the Alfvén waves show a certain degree of dependence on the two-point correlation over  $\sim 200R_E$  between ACE and THEMIS. Alfvén waves with high two-point correlations exhibit a steep spectrum that is associated with a relatively weak wave power above  $2 \times 10^{-4}$  Hz ( $\sim 90$  minutes). By contrast, Alfvén waves with low two-point correlations exhibit a flatter spectrum with a relative enhancement of power above  $2 \times 10^{-4}$  Hz ( $\sim 90$  minutes). Small-scale Alfvénic fluctuations may contribute to the decrease of the two-point correlations over the convection time ( $\sim 1$  hr) of  $\sim 200R_E$ .

The spectral index of Alfvén waves is likely affected by the solar wind speed. The high two-point correlation Alfvén waves with a steeper slope (spectra index  $\sim -1.63$ ) are mostly observed in the low-speed solar wind. This is consistent with the scenario that fluctuations in the slow solar wind are fully developed turbulence with a spectral index close to  $f^{-5/3}$ . The flatter spectrum of the slow solar wind may be due to damping out of the higher-frequency waves between the Sun and 1 au. Alfvén waves with low two-point correlations are distributed equally in high-speed and low-speed solar wind streams. The corresponding spectral index is likely affected by those in the fast streams in which the index may evolve depending on the heliocentric distance. In addition, high two-point correlation Alfvén waves with a steeper slope are found to have a larger angle  $\theta_{BV}$ . The  $\theta_{BV}$  effect may also have made a contribution to the spectral index.

We perform a statistical survey on the geomagnetic responses to the interplanetary Alfvén waves. Alfvén waves in general correspond to a moderate response in the SYM-H, Kp, and SME indices. During the storm time, the responses in Kp, and SME are relatively stronger. The geomagnetic responses show a certain degree of dependence on the two-point correlation and spectra shape of the interplanetary Alfvén waves. Alfvén waves with low two-point correlations and flatter spectra appear to have stronger responses in SYM-H, Kp, and SME.

More Alfvénic power in the spectrum of tens of minutes (30–90 minutes) appears to correspond to stronger geomagnetic responses in our observation. This is consistent with the events studied in Tsurutani et al. (1990) showing that AE-correlated Alfvénic  $B_z$  exhibits enhanced spectra in the range of  $10^{-3}$  to



$10^{-4}$  Hz. Guarnieri et al. (2018) also suggest that 10 minute to 2 hr Alfvén waves cause AE activity and short-scale (<8 minutes) waves are not geoeffective. The 30–90 minute timescale is comparable to the typical 30–60 minute duration of substorm expansion, suggesting a resonance-like relation between Alfvén waves and effective substorm responses (Tsurutani et al. 1990). Longer-period (>90 minutes) Alfvén waves by themselves should be geoeffective. But those long duration (>2 hr) southward  $B_z$  from Alfvén waves only represent a very small portion of all the samples (Figure 5). For many intervals of the AE/SME activity, there are probably no signatures of long-duration (>2 hr) southward  $B_z$  from Alfvén waves (Tsurutani et al. 1995a). In this statistical sense, the geoeffective importance of the 30–90 minute power spectrum is probably more noticeable.

In our observation, the Fourier transform of sharp changes of large  $B_z$  likely contributes to the Alfvénic power spectra in 30–90 minutes and also the higher-frequency band (<10 minutes). Such leakage of power to the higher-frequency band occurs near the sharp changes. In our data, sharp changes in  $B_z$  are expected to be common as a result of phase-steepened large-amplitude Alfvén waves, particularly in the high-speed solar wind streams (Tsurutani et al. 1994, 2018).

The average and non-storm time response indicate that Alfvén waves are generally related to moderate SME increases. Through transient magnetopause reconnection,  $B_z$  from Alfvén waves constantly drives enhanced magnetosphere/ionosphere convection, causing enhanced current flow in the convection AEs and an associated growth of the SME/AE. However, enhanced convection does not necessarily cause substorm expansion (Kamide & Kokubun 1996; Tsurutani et al. 2004). Substorm expansion is more likely to follow if the enhanced convection sufficiently evolves to a certain degree (Kamide et al. 1977; Kan 1993). This is probably the case for many of the storm time Alfvén wave events, in which the evolution of enhanced convection finally leads to substorm expansion, substorm electrojets, and further increases in the SME/AE. Such substorms shall inject energetic particles into the ring current and extend the recovery phase of geomagnetic storms (Tsurutani et al. 2011; Hajra et al. 2014b; Dai et al. 2015b; Hajra & Tsurutani 2018; Raghav et al. 2018; Telloni et al. 2021; Xiong et al. 2022).

We thank NASA CDA web (<https://cdaweb.sci.gsfc.nasa.gov/>), the THEMIS web (<http://themis.ssl.berkeley.edu/>), and the MMS Science Data Center (<https://lasp.colorado.edu/mms/sdc/public/>) for providing the ACE, THEMIS, and MMS data. We appreciate the OMNI database (<https://omniweb.gsfc.nasa.gov/ow.html>) and World Data Center (WDC) for Geomagnetism, Kyoto (<http://wdc.kugi.kyoto-u.ac.jp>) for providing the SYM-H data. We also thank the Johns Hopkins Applied Physics Laboratory for providing the SuperMAG data (<https://supermag.jhuapl.edu/>) and the GFZ German Research Center for Geosciences for providing the Kp index data (<https://www.gfz-potsdam.de/en/kp-index/>). The work at NSSC was supported by NNSFC grants (41731070, 41874175, 42174207), the Specialized Research Fund for State Key Laboratories of China, and the Strategic Pioneer Program on Space Science II, Chinese Academy of Sciences, grants XDA15350201 and XDA15052500. The work at INPE is supported by funds from the China-Brasil Joint Laboratory for Space Weather.

## ORCID iDs

Yimin Han  <https://orcid.org/0000-0003-0097-7818>  
 Lei Dai  <https://orcid.org/0000-0002-5122-3066>  
 Shuo Yao  <https://orcid.org/0000-0003-4267-0486>  
 Chi Wang  <https://orcid.org/0000-0001-6991-9398>  
 Suping Duan  <https://orcid.org/0000-0002-4835-6888>  
 Benoit Lavraud  <https://orcid.org/0000-0001-6807-8494>

## References

- Auster, H. U., Glassmeier, K. H., Magnes, W., et al. 2008, *SSRv*, **141**, 235  
 Baumjohann, W., & Treumann, R. A. 1996, *Basic Space Plasma Physics* (London: Imperial College Press)  
 Bavassano, B., Dobrowolny, M., Mariani, F., & Ness, N. F. 1982, *JGR*, **87**, 3617  
 Belcher, J. W., & Davis, L. J. 1971, *JGR*, **76**, 3534  
 Belcher, J. W., Davis, L. J., Leverett, J., & Smith, E. J. 1969, *JGR*, **74**, 2302  
 Bieber, J. W., Wanner, W., & Matthaeus, W. H. 1996, *JGR*, **101**, 2511  
 Borovsky, J. E., & Denton, M. H. 2010, *JGRA*, **115**, A10101  
 Bruno, R., Bavassano, B., D’Amicis, R., et al. 2006, *SSRv*, **122**, 321  
 Bruno, R., Carbone, V., Sorriso-Valvo, L., & Bavassano, B. 2003, *JGRA*, **108**, 1130  
 Chian, A. C.-L., Kamide, Y., Rempel, E. L., & Santana, W. M. 2006, *JGRA*, **111**, A07S03  
 Dai, L., Han, Y., Yao, S., et al. 2023, *ApJ*, **945**, 47  
 Dai, L., Takahashi, K., Lysak, R., et al. 2015a, *JGRA*, **120**, 4748  
 Dai, L., Wang, C., Duan, S., et al. 2015b, *GeoRL*, **42**, 6170  
 Dai, L., Wang, C., Cai, Z., et al. 2020, *FrP*, **8**, 89  
 Dai, L., Wygant, J. R., Cattell, C. A., et al. 2014, *GeoRL*, **41**, 1398  
 D’Amicis, R., Bruno, R., & Bavassano, B. 2007, *GeoRL*, **34**, L05108  
 Denskat, K., & Burlaga, L. 1977, *JGR*, **82**, 2693  
 Denskat, K., & Neubauer, F. 1982, *JGRA*, **87**, 2215  
 Diego, P., Storini, M., Parisi, M., & Cordaro, E. G. 2005, *JGRA*, **110**, A06105  
 Farrugia, C. J., Matsui, H., Kucharek, H., et al. 2005, *JGRA*, **110**, A09S13  
 Gonzalez, W. D., Joselyn, J. A., Kamide, Y., et al. 1994, *JGR*, **99**, 5771  
 Gonzalez, W. D., Tsurutani, B. T., & Clúa de Gonzalez, A. L. 1999, *SSRv*, **88**, 529  
 Guarnieri, F. L., Tsurutani, B. T., Vieira, L. E. A., et al. 2018, *NPGEO*, **25**, 67  
 Hajra, R., Echer, E., Tsurutani, B. T., & Gonzalez, W. D. 2013, *JGRA*, **118**, 5626  
 Hajra, R., Echer, E., Tsurutani, B. T., & Gonzalez, W. D. 2014a, *JGRA*, **119**, 2675  
 Hajra, R., Tsurutani, B. T., Echer, E., & Gonzalez, W. D. 2014b, *GeoRL*, **41**, 1876  
 Hajra, R., & Tsurutani, B. T. 2018, in *Extreme Events in Geospace*, ed. N. Buzulukova (Amsterdam: Elsevier), 373  
 Horbury, T. S., Forman, M., & Oughton, S. 2008, *PhRvL*, **101**, 175005  
 Horbury, T. S., Forman, M. A., & Oughton, S. 2005, *PPCF*, **47**, B703  
 Kamide, Y., Baumjohann, W., Daglis, I. A., et al. 1998, *JGR*, **103**, 17705  
 Kamide, Y., & Kokubun, S. 1996, *JGRA*, **101**, 13027  
 Kamide, Y., Perreault, P., Akasofu, S.-I., & Winningham, J. 1977, *JGR*, **82**, 5521  
 Kan, J. 1993, *JGRA*, **98**, 17263  
 Kennel, C. F. 1996, *Convection and Substorms—Paradigms of Magnetospheric Phenomenology*, Vol. 2 (New York: Oxford Academic)  
 Koga, D., Gonzalez, W., Souza, V., et al. 2019, *JGRA*, **124**, 8778  
 Lee, D. Y., Lyons, L. R., Kim, K. C., et al. 2006, *JGRA*, **111**, A12214  
 Li, H., Li, N., Wang, C., & Yao, S. 2020, *ApJL*, **889**, L16  
 Lu, Q., Hu, Q., & Zank, G. P. 2009, *ApJ*, **706**, 687  
 Matzka, J., Stolle, C., Yamazaki, Y., Bronkalla, O., & Morschhauser, A. 2021, *SpWea*, **19**, e2020SW002641  
 McComas, D. J., Bame, S. J., Barker, P., et al. 1998, *SSRv*, **86**, 563  
 McFadden, J. P., Carlson, C. W., Larson, D., et al. 2008, *SSRv*, **141**, 277  
 McKenzie, J. F., & Westphal, K. O. 1969, *P&SS*, **17**, 1029  
 Newell, P. T., & Gjerloev, J. W. 2011, *JGRA*, **116**, A12211  
 Phan, T., Paschmann, G., Gosling, J., et al. 2013, *GeoRL*, **40**, 11  
 Pytte, T., McPherron, R., Hones, E., Jr., & West, H., Jr. 1978, *JGRA*, **83**, 663  
 Raab, W., Branduardi-Raymont, G., Wang, C., et al. 2016, *Proc. SPIE*, **9905**, 990502  
 Raghav, A. N., Kule, A., Bhaskar, A., et al. 2018, *ApJ*, **860**, 26  
 Richardson, J., Dashevskiy, F., & Paularena, K. 1998, *JGRA*, **103**, 14619  
 Richardson, J. D., & Paularena, K. I. 2001, *JGRA*, **106**, 239  
 Russell, C. T., Siscoe, G. L., & Smith, E. J. 1980, *GeoRL*, **7**, 381  
 Shi, M. J., Xiao, C. J., Li, Q. S., et al. 2015, *ApJ*, **815**, 122

- Sibeck, D. G., Angelopoulos, V., Brain, D. A., et al. 2011, *SSRv*, **165**, 59
- Smith, C. W., L'Heureux, J., Ness, N. F., et al. 1998, *SSRv*, **86**, 613
- Smith, E., Balogh, A., Neugebauer, M., & McComas, D. 1995, *GeoRL*, **22**, 3381
- Swisdak, M., Rogers, B., Drake, J., & Shay, M. 2003, *JGRA*, **108**, 1218
- Telloni, D., D'Amicis, R., Bruno, R., et al. 2021, *ApJ*, **916**, 64
- Tsurutani, B. T., Echer, E., Guarnieri, F. L., & Gonzalez, W. D. 2011, *JASTP*, **73**, 164
- Tsurutani, B. T., & Gonzalez, W. D. 1987, *P&SS*, **35**, 405
- Tsurutani, B. T., Gonzalez, W. D., Gonzalez, A. L. C., et al. 1995a, *JGRA*, **100**, 21717
- Tsurutani, B. T., Ho, C. M., Arballo, J. K., Goldstein, B. E., & Balogh, A. 1995b, *GeoRL*, **22**, 3397
- Tsurutani, B. T., Gonzalez, W. D., Guarnieri, F., et al. 2004, *JASTP*, **66**, 167
- Tsurutani, B. T., Gould, T., Goldstein, B. E., Gonzalez, W. D., & Sugiura, M. 1990, *JGR*, **95**, 2241
- Tsurutani, B. T., Ho, C. M., Smith, E. J., et al. 1994, *GeoRL*, **21**, 2267
- Tsurutani, B. T., Lakhina, G. S., Sen, A., et al. 2018, *JGRA*, **123**, 2458
- Tu, C.-Y., & Marsch, E. 1995, *SSRv*, **73**, 1
- Tu, C.-Y., Marsch, E., & Thieme, K. 1989, *JGRA*, **94**, 11739
- Wang, C., & Branduardi-Raymond, G. 2018, *ChJSS*, **38**, 657
- Wang, X., Tu, C., Wang, L., He, J., & Marsch, E. 2015, *GeoRL*, **42**, 3654
- Wanliss, J. A., & Showalter, K. M. 2006, *JGRA*, **111**, A02202
- Xiong, S., Dai, L., Wang, C., et al. 2022, *JGRA*, **127**, e30088
- Zhang, X. Y., Moldwin, M. B., Steinberg, J. T., & Skoug, R. M. 2014, *JGRA*, **119**, 3259
- Zong, Q.-G., Yue, C., & Fu, S.-Y. 2021, *SSRv*, **217**, 33